

Structure and dimensionality of coordination complexes correlated to piperazine conformation: from discrete $[\text{Cu}^{\text{II}}_2]$ and $[\text{Cu}^{\text{II}}_4]$ complexes to a $\mu_{1,3}\text{-N}_3^-$ bridged $[\text{Cu}^{\text{II}}_2]_n$ chain†

Alok Ranjan Paital,^a Debashree Mandal,^a Xiaoying Huang,^b Jing Li,^b Guillem Aromí^{*c} and Debashis Ray^{*a}

Received 22nd August 2008, Accepted 24th November 2008

First published as an Advance Article on the web 9th January 2009

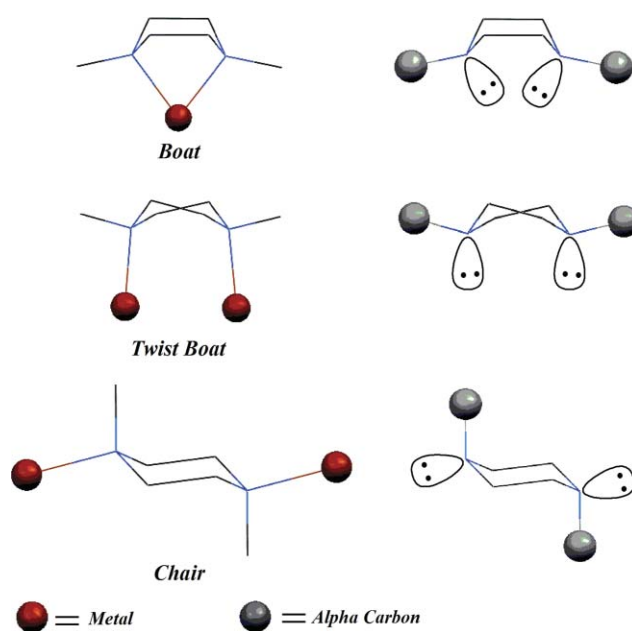
DOI: 10.1039/b814681k

Three different types of copper(II) complexes have been studied of the hexadentate Schiff base ligand *N,N'*-bis[2-((salicylideneimine)amino)ethyl] piperazine (H_2L) having the piperazine backbone in the chair form and axial–axial (a,a) N-atom lone pairs in the free state. The structure of the products is influenced by the reaction conditions and by the exogenous ligands, affecting the conformation of the piperazine moiety (primary structure) and the topology and nuclearity of the resulting complexes (secondary structure). In $[\text{Cu}_2\text{L}(\text{DMF})_2]\text{X}_2$ ($\text{X} = \text{ClO}_4^-$, **1a**; NO_3^- , **1b**), the lone-pairs of chair-piperazine adopt the equatorial–equatorial (e,e) conformation. In the presence of NEt_3 and NaN_3 , two types of $[\text{Cu}^{\text{II}}_4]$ complexes $[\text{Cu}_4(\text{L})_2(\text{OH})_2(\text{H}_2\text{O})_2]\text{X}_2 \cdot n\text{H}_2\text{O}$ ($\text{X} = \text{ClO}_4^-$, $n = 1$, **2a**; $\text{X} = \text{NO}_3^-$, $n = 4$, **2b**) and $[\text{Cu}_4(\text{L})_2(\text{N}_3)_2(\text{H}_2\text{O})_2]\text{X}_2 \cdot \text{H}_2\text{O}$ ($\text{X} = \text{ClO}_4^-$, **3a**; NO_3^- , **3b**) are obtained where four copper(II) ions are bridged by two hexadentate μ_3 -piperazine ligands, this time in chair–e,a conformation, and by two OH and N_3 groups. In CH_3CN , reactions of **1**, **2** or **3** with NaN_3 always produce the double end-to-end azido bridged 1D polymer $[\text{Cu}_2\text{L}(\text{N}_3)_2]_n$ (**4**) having a chair–e,e piperazine backbone. All studied conformations of the piperazine bridge mediate antiferromagnetic interactions between the Cu(II) ions, as revealed by bulk magnetization measurements. The striking difference in intensity of the coupling through *trans*-e,e piperazine observed for complexes **1a** and **4** might be due to complementarily effects between the ligands involved.

Introduction

The synthesis and characterization of metal–organic frameworks (MOFs) based on coordination chemistry continues to be of great current interest to a variety of disciplines. Among these is molecular magnetism, where such kind of studies have allowed, for instance, to establish magneto-structural correlations,¹ exploit cooperativity in spin crossover systems² or aim at multifunctional materials.³ Among the criteria for choosing the appropriate ligands in this context is the ability to control the topology of the assembly and the directionality of the framework growth, perhaps as a function of the reaction conditions or the presence of other co-ligands. In this regard, substituted piperazine-based ligands are of particular interest, since they can adopt various conformations and thus engage its donor atoms in sets of coordination bonds with different directions,^{4–6} thereby offering the possibility of controlling the geometry of the resulting metal complexes. More precisely, the piperazine moiety can have four distinct conformations: chair, boat, twist-boat and half-boat,⁷ of which the former is the most

favorable thermodynamically. The first three forms have been established crystallographically in metal complexes (Scheme 1). In the boat and twist-boat forms, the piperazine unit chelates one, or bridges, two metal ions to give the mono^{7–10} and dinuclear^{11,12} complexes, respectively. When in the chair conformation, the unit has been usually found to bridge pairs of metals in a *trans*-*N,N'*



Scheme 1

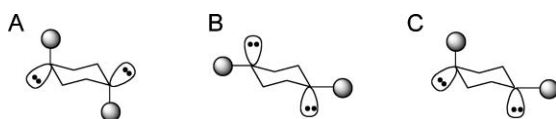
^aDepartment of Chemistry, Indian Institute of Technology, Kharagpur 721 302, India

^bDepartment of Chemistry and Chemical Biology, Rutgers University, Piscataway 08854, NJ, USA

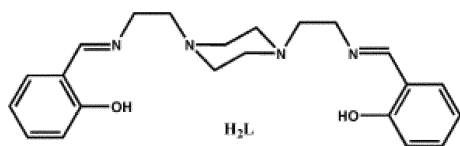
^cDepartament de Química Inorgànica, Universitat de Barcelona, Diagonal, 647, 08028 Barcelona, Spain

† Electronic supplementary information (ESI) available: Synthesis scheme, FTIR spectra, hydrogen bonding figure and structural figures. CCDC reference numbers 236808, 642073, 275431, 642074 and 601654. For ESI and crystallographic data in CIF or other electronic format see DOI: 10.1039/b814681k

configuration, either in the equatorial–equatorial (e,e) or the axial–axial (a,a) fashion (Scheme 2, A and B).^{13,14} Only recently, in a preliminary communication of this work, we reported a rare example of *cis-N,N'* coordination of the ‘chair’ piperazine (thus in the a,e mode; Scheme 2, C) within a [Cu₄] complex.¹⁵ The e,e mode of the *trans-N,N'* bridging fashion usually facilitates the formation of polymeric structures.^{16,17} Herein, we report a series of Cu^{II} complexes involving the Schiff-base piperazine ligand H₂L (Scheme 3) and various exogenous bridging groups. This series of compounds show that progressive changes in reaction conditions lead to stabilization of systems with similar composition and basic [Cu(μ-L)] structural motif but dramatically different nuclearity or dimensionality (secondary structure of the complex). These drastic changes in overall geometry are in part permitted thanks to the conformational versatility of the piperazine moiety (primary structure of the assembly), and to the fact that the various conformers are kinetically accessible. The structure and properties of these new complexes are described.



Scheme 2



Scheme 3

Experimental

Materials and physical measurements

The elemental analyses (C, H and N) were performed with a Perkin-Elmer model 240 C elemental analyzer. Copper analysis was performed volumetrically following a standard iodometric titration method.¹⁸ IR spectra were recorded on a Perkin-Elmer 883 spectrophotometer. The solution electrical conductivity and electronic spectra were obtained using a Unitech type U131C digital conductivity meter with a solute concentration of about 10⁻³ M and a Shimadzu UV 1601 UV-vis-NIR spectrophotometer, respectively. Magnetic measurements were carried out in the ‘‘Servei de Magnetoquímica (Universitat de Barcelona)’’ on polycrystalline samples (*ca.* 30 mg) using a Quantum Design MPMS XL-5 SQUID susceptometer operating at a constant magnetic field of 1 T between 2–300 K. The experimental magnetic moment was corrected for the diamagnetic contribution from the sample holder and the diamagnetic response from the sample, which was evaluated from Pascal’s constants.

Syntheses

2-[4-(2-Amino-ethyl)-piperazine-1-yl]ethylamine was prepared by a reported procedure.¹⁹ Cupric perchlorate hexahydrate was prepared by treating copper(II) carbonate with 1 : 1 HClO₄

and crystallized after concentration in a water bath. All other chemicals and solvents were reagent grade materials and were used as received without further purification.

Caution! Azide derivatives are potentially explosive, only a small amount of materials should be prepared, and they should be handled with proper care.

1,4-Bis(2-salicylideneaminoethyl) piperazine (H₂L). To the methanolic solution (30 mL) of 2-[4-(2-amino-ethyl)-piperazine-1-yl]ethylamine (1 g, 5.8 mmol), salicylaldehyde (1.211 mL, 11.6 mmol) was added under ice-cold conditions and stirred for 3 h to give a yellow solid, which was separated by filtration through a G4 sintered bed and washed thoroughly with hexane and water. Finally, the isolated compound was dried *in vacuo* over P₄O₁₀. The single crystals suitable for X-ray analysis were obtained from hot MeOH during 4 d and found to be same as reported earlier.¹⁹ Yield 1.92 g (~87%), mp 152 °C. Anal. calcd for C₂₂H₂₈N₄O₂: C 69.44, H 7.42, N 14.72. Found: C 69.22, H 7.12, N 14.68. IR (KBr) ν/cm⁻¹: 2939 (b), 2823 (b), 1641 (vs), 1499 (s), 1441 (s), 1281 (vs), 1159 (s), 1017 (s), 863 (s), 764 (s). ¹H NMR (CDCl₃) δ/ppm: (phenolic OH) 13.43 (s, 2H), 8.35 (s, 2H), 7.35–6.83 (m, 8H), 3.73 (t, 4H), 2.70 (t, 4H), 2.57 (s, 8H). ¹³C NMR (CDCl₃) δ/ppm: (C_{7,16}) 165.52, (C_{1,22}) 161.16, (C_{6,17}) 132.13, (C_{3,5,18,20}) 131.14, (C_{4,19}) 118.44, (C_{2,21}) 116.98, (C_{9,14}) 58.59, (C_{8,15}) 56.98, (C_{10,11,12,13}) 53.33.

[Cu₂L(DMF)₂](ClO₄)₂ (1a). To a solution of H₂L (0.5 g, 1.31 mmol) in CHCl₃–MeOH (1 : 1 v/v, 30 mL) was added Cu(ClO₄)₂·6H₂O (0.97 g, 2.62 mmol) in MeOH (20 mL), followed by the addition of Et₃N (0.36 mL, 2.62 mmol). The mixture was stirred for 1 h, and a green solid was obtained as a precipitate. The solid was isolated, washed with cold methanol, and dried under vacuum over P₄O₁₀. The above solid was recrystallized from DMF and obtained in 80% yield after 1 week, in the form of crystals suitable for X-ray crystallography. Anal. calcd for C₂₈H₄₀Cl₂Cu₂N₆O₁₂: C 39.53, H 4.74, N 9.88, Cu 14.95%. Found: C 39.48, H 4.96, N 9.77, Cu 14.48%. IR (KBr) ν/cm⁻¹: 3435 (b), 1615 (vs), 1535 (s), 1434 (s), 1400 (s), 1314 (s), 1085 (s). Molar conductance, (DMF solution) A_M/ohm⁻¹cm²mol⁻¹: 145. UV-vis (DMF solution) (λ_{max}/nm (ε/L mol⁻¹cm⁻¹)): 589 (266), 370 (7169), 306 (11 500), 271 (21 551).

[Cu₂L(DMF)₂](NO₃)₂ (1b). This complex was synthesized by following the above procedure using Cu(NO₃)₂·3H₂O (0.63 g, 1.31 mmol). Anal. calcd for C₂₈H₄₀Cu₂N₈O₁₀: C 43.35, H 5.20, N 14.44, Cu 16.38%. Found: C 43.21, H 5.18, N 14.28, Cu 16.22%. IR (KBr) ν/cm⁻¹: 3428 (b), 1635 (s), 1600 (m), 1447 (m), 1385 (vs), 1198 (m), 911 (m), 769 (m). Molar conductance, (DMF solution) A_M/ohm⁻¹cm²mol⁻¹: 130. UV-vis (DMF solution) (λ_{max}/nm (ε/L mol⁻¹cm⁻¹)): 617 (338), 376 (8200), 308 (12 200), 271 (22 150).

[Cu₄(L)₂(OH)₂(H₂O)₂](ClO₄)₂·H₂O (2a·H₂O). To a solution of H₂L (0.5 g, 1.31 mmol) in CHCl₃–MeOH (1 : 1 v/v, 30 mL) was added Et₃N (0.55 mL, 3.93 mmol) and a solution of Cu(ClO₄)₂·6H₂O (0.97 g, 2.62 mmol) in MeOH (20 mL). The mixture was stirred for 1 h, and a complex precipitated then as a green solid (~85% yield). The solid was isolated, washed with cold methanol, and dried under vacuum over P₄O₁₀. Single crystals suitable for X-ray analysis were obtained from 1 : 1 (v/v) MeOH–CHCl₃ after 6 d. Anal. calcd for C₄₄H₆₀Cl₂Cu₄N₈O₁₇: C 40.71, H 4.66, N 8.63, Cu 19.57%. Found: C 40.64, H 4.55, N 8.48, Cu 19.05%. IR (KBr) ν/cm⁻¹: 3415 (vs), 1634 (vs), 1454

(m), 1287 (m), 1210 (w), 1107 (vs), 907 (w), 766 (m), 625 (m). Molar conductance, (MeCN solution) $A_M/\text{ohm}^{-1}\text{cm}^2\text{mol}^{-1}$: 220. UV-vis (MeCN solution) ($\lambda_{\text{max}}/\text{nm}$ ($\epsilon/\text{L mol}^{-1}\text{cm}^{-1}$)): 605 (447), 376 (11 489), 323 (17 849), 274 (32 965).

[Cu₄(L)₂(OH)₂(H₂O)₂](NO₃)₂·4H₂O (2b·4H₂O). This complex was synthesized by following the above procedure using Cu(NO₃)₂·3H₂O (0.63 g, 2.61 mmol). Anal. calcd for C₄₄H₆₆Cu₄N₁₀O₁₈: C 41.38, H 5.21, N 10.97, Cu 19.90%. Found: C 41.22, H 5.28, N 10.76, Cu 19.86%. IR (KBr) ν/cm^{-1} : 3420 (b), 1635 (s), 1600 (m), 1448 (m) 1384 (vs), 1198 (m), 767 (m). Molar conductance, (CH₃CN solution) $A_M/\text{ohm}^{-1}\text{cm}^2\text{mol}^{-1}$: 218. UV-vis (MeCN solution) ($\lambda_{\text{max}}/\text{nm}$ ($\epsilon/\text{L mol}^{-1}\text{cm}^{-1}$)): 590 (482), 372 (18 172), 318(15 121), 271(22 704), 227(29 700).

[Cu₄(L)₂(N₃)₂(H₂O)₂](ClO₄)₂·H₂O (3a·H₂O). To a solution of Cu(ClO₄)₂·6H₂O (0.97 g, 2.62 mmol) in MeOH (15 mL) was added for 15 min under stirring another solution of NaN₃ (0.085 g, 1.31 mmol) in MeOH (15 mL). Then, a solution of H₂L (0.5 g, 1.31 mmol) in CHCl₃–MeOH (1 : 1 v/v, 30 mL) was added to the above mixture followed by addition of Et₃N (0.36 mL, 2.611 mmol). The system was stirred for 1 h and produced a green precipitate. The solid was isolated, washed with cold methanol, and dried under vacuum over P₄O₁₀. The yield was 75%. Anal. calcd for C₄₄H₅₈Cl₂Cu₄N₁₄O₁₅: C 39.20, H 4.34, N 14.55, Cu 18.85%. Found: C 39.24, H 4.18, N 14.22, Cu 18.76%. IR (KBr) ν/cm^{-1} : 3420 (vs), 2077 (vs), 1634 (vs), 1600 (m), 1539 (m), 1448 (m), 1310 (m), 1093 (vs), 765 (m), 623 (m). Molar conductance, (MeCN solution) $A_M/\text{ohm}^{-1}\text{cm}^2\text{mol}^{-1}$: 240. UV-vis (MeCN solution) ($\lambda_{\text{max}}/\text{nm}$ ($\epsilon/\text{L mol}^{-1}\text{cm}^{-1}$)): 598 (875), 373 (16 215), 309 (18 385), 274 (29 165).

[Cu₄(L)₂(N₃)₂(H₂O)₂](NO₃)₂·H₂O (3b·H₂O). This complex was synthesized by following the above procedure using Cu(NO₃)₂·3H₂O (0.63 g, 2.61 mmol). The yield was 73%. Anal. calcd for C₄₄H₅₈Cu₄N₁₆O₁₃: C 41.51, H 4.59, N 17.60, Cu 19.96%. Found: C 41.42, H 4.62, N 17.48, Cu 19.88%. IR (KBr) ν/cm^{-1} : 3436 (b), 2049 (vs), 1637 (s), 1449 (m) 1384 (vs), 763 (m). Molar conductance, (DMF solution) $A_M/\text{ohm}^{-1}\text{cm}^2\text{mol}^{-1}$: 145. UV-vis (DMF solution) ($\lambda_{\text{max}}/\text{nm}$ ($\epsilon/\text{L mol}^{-1}\text{cm}^{-1}$)): 607 (863), 372 (16 102), 302 (14 587), 277(26 377).

[Cu₂L(N₃)₂]_n (4).

Method 1. To a solution of H₂L (0.5 g, 1.31 mmol) and Et₃N (0.36 ml, 2.62 mmol) in CHCl₃–MeOH (1 : 1 v/v, 30 mL) was added a solution of Cu(ClO₄)₂·6H₂O (0.97 g, 2.62 mmol) MeCN–MeOH (1 : 1 v/v, 30 mL). The mixture was stirred for 15 min and then a solution of NaN₃ (0.170 g, 2.62 mmol) in MeOH (10 mL) was added. The mixture was stirred for a further 1 h to give a green precipitate. The solid was isolated, washed with cold methanol–water and dried under vacuum over P₄O₁₀. The yield was 85%. Single crystals suitable for X-ray analysis were obtained from MeCN after one week. Anal. calcd for C₂₂H₂₆Cu₂N₁₀O₂: C 44.81, H 4.44, N 23.75, Cu 21.55%. Found: C 44.72, H 4.52, N 23.68%. IR (KBr) ν/cm^{-1} : 2061 (vs), 1634 (vs), 1600 (m), 1530 (m), 1448 (s), 1353 (m), 1196 (m), 770 (m), 754 (m). Molar conductance, (DMF solution) $A_M/\text{ohm}^{-1}\text{cm}^2\text{mol}^{-1}$: 6. UV-vis (MeCN solution) ($\lambda_{\text{max}}/\text{nm}$ ($\epsilon/\text{L mol}^{-1}\text{cm}^{-1}$)): 600 (540), 372 (11 735), 308 (11 596), 272 (28 328).

Method 2. To a DMF (10 mL) solution of complex **1a/1b** (0.425/0.387 g; 0.5 mmol), was added slowly a solution of NaN₃

(0.065 g, 1 mmol) in MeOH (10 mL) and the mixture was stirred for 30 min, yielding a greenish precipitate of complex **4**. The solid was isolated, washed with cold methanol–water and dried under vacuum over P₄O₁₀. All analytical data and spectroscopic characterization indicates the formation of complex **4**.

Method 3. To a MeCN (10 mL) solution of complex **2a/2b** (0.389/0.383 g; 0.3 mmol), was added slowly a solution of NaN₃ (0.078 g, 1.2 mmol) in MeOH (10 mL) and the mixture was stirred for 30 min to yield a greenish precipitate of **4**. The solid was isolated, washed with cold methanol–water and dried under vacuum over P₄O₁₀. All analytical data and spectroscopic characterization indicate formation of **4**.

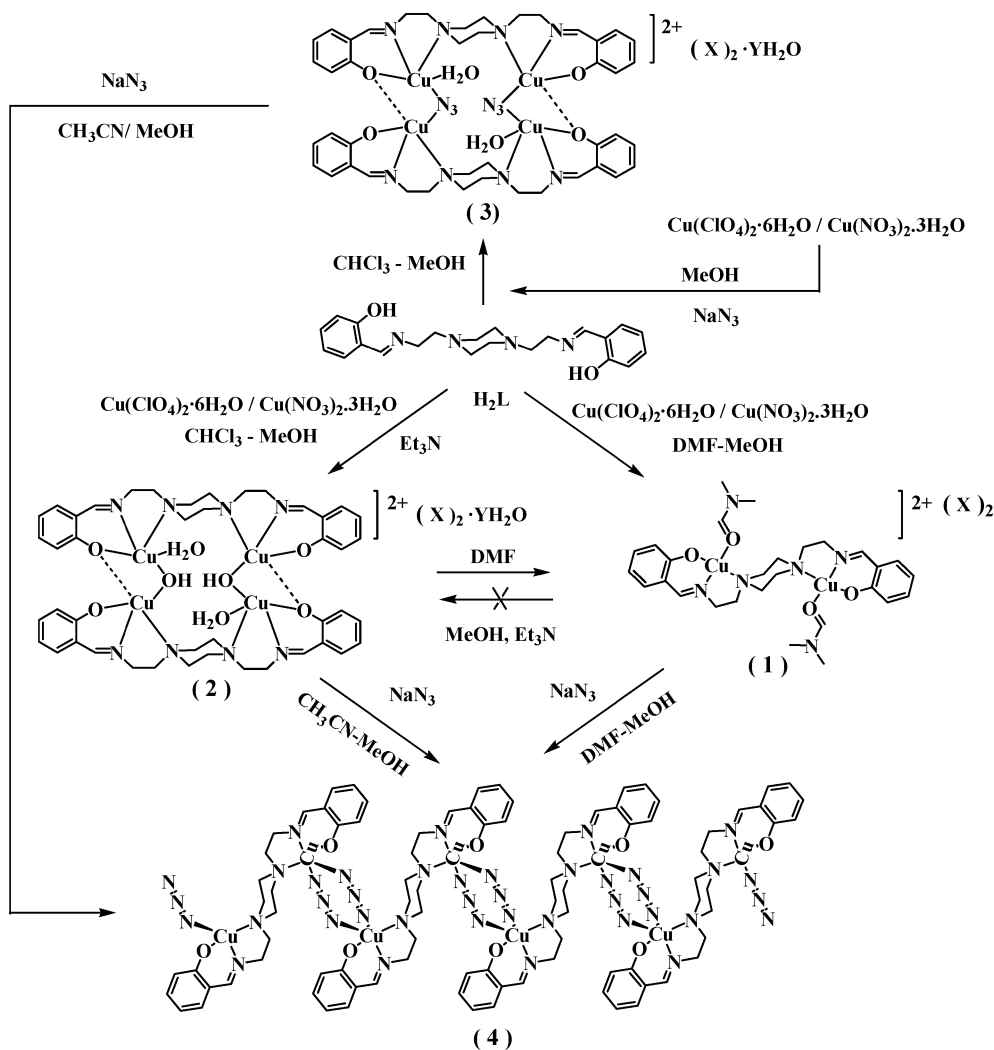
Method 4. To a MeCN–DMF (1 : 1 v/v, 20 mL) solution of complex **3a/3b** (0.404/0.381 g; 0.3 mmol), was added slowly a solution of NaN₃ (0.039 g, 0.6 mmol) in MeOH (5 mL) and the mixture was stirred for 30 min to yield a greenish precipitate of **4**. The solid was isolated, washed with cold methanol–water and dried under vacuum over P₄O₁₀. All analytical data and spectroscopic characterizations support formation of complex **4**.

Results and discussion

Synthesis and characterization

The ligand H₂L is prepared (Scheme S1)† from the appropriate piperazine diamine, from its reaction with 2 mol of salicylaldehyde, in 87% yield.¹⁵ The molecule has been fully characterized (see Experimental) and its single-crystal X-ray diffraction structure reveals that the piperazine backbone exists in the chair-a, a conformation (Scheme 2, B), *i.e.*, with the nitrogen lone pairs available for metal ion coordination axially directed. The coordination behaviour of this piperazine containing ligand is expected to be distinct from the analogous hexadentate donor, where the cyclic amine is replaced by an ethylenediamine bridge.²⁰ In particular, the piperazine moiety confers a higher rigidity to the ligand, decreasing the degrees of freedom to the structure of possible ensuing metal complexes.

Reactions of H₂L with Cu(ClO₄)₂ or Cu(NO₃)₂ in a DMF–MeOH solvent mixture containing NEt₃ (1 : 2 : 2 molar ratio) led upon slow evaporation to crystals of [Cu₂L(DMF)₂]₂X₂ (**1**) (X = ClO₄⁻, **1a**; NO₃⁻, **1b**) in high yield (Scheme 4). Complex **1a** had been previously obtained by us through a different route, resulting from *in situ* transformation of an imidazolidine ligand.¹³ In contrast to the above, the same reactions performed in CHCl₃–MeOH (Scheme 4) produced the tetranuclear complexes [Cu₄(L)₂(OH)₂(H₂O)₂]₂X₂·nH₂O (X = ClO₄⁻, n = 1, **2a**·H₂O; X = NO₃⁻, n = 4, **2b**·4H₂O) directly from the reaction mixture, also in high yield (optimized for the 1 : 6 : 2 molar ratio). The procedure used for the preparation of complexes of type **2** was repeated employing the salt NaN₃ instead of the base NEt₃. The products this time are proposed to be [Cu₄(L)₂(N₃)₂(H₂O)₂]₂X₂·H₂O (**3**·H₂O) (X = ClO₄⁻, **3a**; NO₃⁻, **3b**) and were obtained in high yields as optimized using stoichiometric amounts of the reactants. Elemental analysis and conductivity measurements together with UV-vis spectroscopy and IR spectroscopy were used to fully characterize these compounds, and were consistent with the above formulations. The IR C=N stretching frequencies of **1a** and **1b** appear at 1615 and 1635 cm⁻¹, respectively, whereas strong bands corresponding to the ClO₄⁻ and NO₃⁻ show up at 1085 and



Compound	X	Y
1a	ClO ₄ ⁻	
1b	NO ₃ ⁻	
2a	ClO ₄ ⁻	1
2b	NO ₃ ⁻	4
3a	ClO ₄ ⁻	1
3b	NO ₃ ⁻	1

Scheme 4

1385 cm⁻¹, respectively. The infrared spectra of **2a** and **2b** also show essentially the same distinctive features, in addition to bands at 3415 and 3420 cm⁻¹, respectively, corresponding to O–H stretching frequencies from lattice water molecules. The infrared spectra of **3a** and **3b** exhibit the bands expected for the C=N, ClO₄⁻ (or NO₃⁻) moieties and –OH moieties (see Experimental), in addition to strong signals at 2077 and 2049 cm⁻¹, respectively, confirming the presence of N₃⁻ ligands (Fig. S1).[†] In the absence of single-crystal X-ray diffraction studies, the formation of compounds of type **3** is supported by the observation of the analogous complexes of type **2** (Scheme 4).

The differences in identity and structure of compounds **1a** and **1b** with respect to **2a** and **2b** are striking. These underline once again the fact that solvents may not be innocent media with regard to the topology of the product of a reaction in coordination chemistry. Interestingly, we observed that **2a** and **2b**, which are stable in MeOH and CH₃CN, produce complexes **1a** and **1b**, respectively, upon recrystallization from DMF, as confirmed from the cell parameters of the corresponding single crystals. Remarkable solvent-induced changes of structure and nuclearity have been previously observed.²¹ In this case, the transformation requires a change of conformation of the piperazine moiety from

trans-e,e to *cis-a,e*, which indicates that this conversion occurs freely in solution at room temperature. This suggests that the formation of complexes **2a** and **2b** may occur after the initial formation of a dinuclear entity of the type $[\text{Cu}_2\text{L}(\text{H}_2\text{O})_n]$ ($n = 2-4$) similar to the cation of **1**, followed by the dimerization into the tetranuclear entity with help of the base (Scheme S2).[†] This aggregation needs to occur while the dimeric fractions are in the *cis* form.

Both dinuclear (**1a** and **1b**) and tetranuclear (**2a**, **2b**, **3a** and **3b**) complexes react with the stoichiometric amount of NaN_3 in DMF–MeOH and MeCN–MeOH, respectively, to form the 1D zigzag chain complex $[\text{Cu}_2\text{L}(\text{N}_3)_2]_n$ (**4**) (see below), exclusively, in high yield (Scheme 4). These transformations imply either a change of conformation of the chair-piperazine group or the conservation of the *trans-a,a* conformation. It is not clear whether or not the latter is the main reason for the preference for the polymeric arrangement rather than a discrete tetranuclear array with double N_3^- bridges.²² The IR spectrum of **4** revealed a band at 2061 cm^{-1} , characteristic of the azide ligand.

Description of structures

$[\text{Cu}_2\text{L}(\text{DMF})_2]\text{X}_2$ (**1**) ($\text{X} = \text{ClO}_4$, **1a**; NO_3 , **1b**). Complexes **1a** and **1b** crystallize in the $P\bar{1}$ space group and contain both the same complex cation, $[\text{Cu}_2\text{L}(\text{DMF})_2]^{2+}$ (Fig. 1), together with perchlorate (**1a**) or nitrate (**1b**) anions where complex **1a** has been reported earlier.¹³ Crystallographic data are in Table 1, while selected bond distances and angles are given in Table 2. The complex cation contains two square planar Cu(II) ions bridged and chelated by the hexadentate piperazine ligand L^{2-} . In this assembly, the piperazine moiety of L^{2-} exhibits the chair conformation and the coordination occurs in the *trans-e,e* fashion. This means that the ligand, which in the solid-state is found in

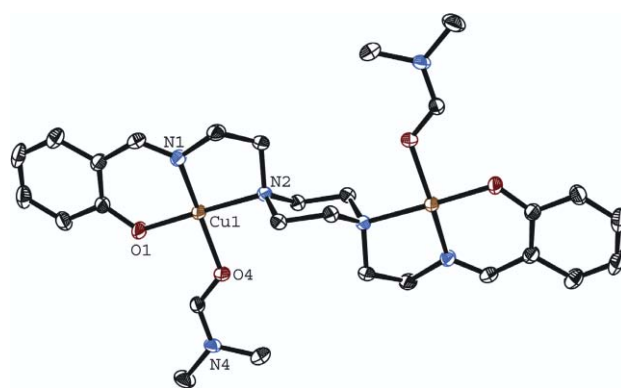


Fig. 1 ORTEP view at 30% probability level of the $[\text{Cu}_2\text{L}(\text{DMF})_2]^{2+}$ cation of **1b** (the analogous cation for **1a** is virtually identical). Hydrogen atoms are omitted for clarity.

the *a,a* configuration, undergoes a conformational change of its backbone upon coordination. Each copper ion in the complex is coordinated by one phenoxide, one imine and one piperazine amine from L^{2-} . The remaining equatorial site on each copper center is occupied by the oxygen atom of one molecule of DMF, completing the *cis*- N_2O_2 square coordination environment around the metals. The electro-neutrality of the system is ensured by the presence of two counter ions (either ClO_4^- or NO_3^-), which are weakly coordinated to the Cu(II) centers through long axial (pseudo) bonds, exhibiting distances of 2.67 and 2.45 Å, for **1a** (ClO_4^-) and **1b** (NO_3^- , see Fig. 2), respectively. The $\text{Cu}-\text{N}_{\text{im}}$ distances (involving $\text{sp}^2\text{ N}$) are slightly shorter than the $\text{Cu}-\text{N}_{\text{am}}$ distances (involving $\text{sp}^3\text{ N}$), whereas the $\text{Cu}-\text{O}_{\text{ph}}$ bond lengths exhibit smaller values than the $\text{Cu}-\text{O}_{\text{DMF}}$ distances (Table 2). The distance of Cu(II) from the idealized equatorial plane is 0.09 Å in **1a**, shorter than for **2a** (0.17 Å), presumably because the fact

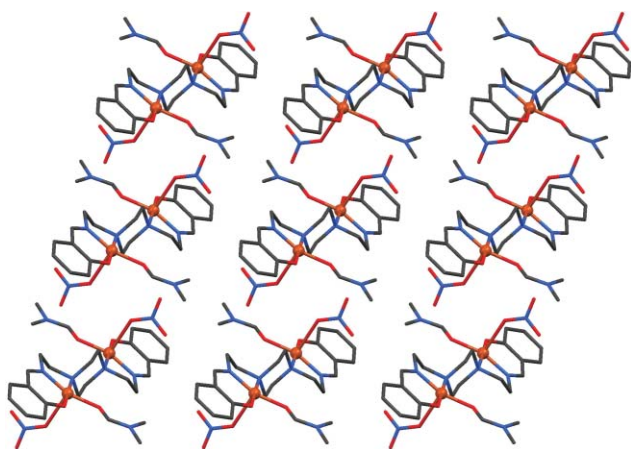
Table 1 X-Ray crystallographic data

	1a	1b	2a	2b	4
Molecular formula	$\text{C}_{28}\text{H}_{40}\text{Cl}_2\text{Cu}_2\text{N}_6\text{O}_{12}$	$\text{C}_{28}\text{H}_{40}\text{Cu}_2\text{N}_8\text{O}_{10}$	$\text{C}_{44}\text{H}_{60}\text{Cl}_2\text{Cu}_4\text{N}_8\text{O}_{17}$	$\text{C}_{44}\text{H}_{66}\text{Cu}_4\text{N}_{10}\text{O}_{18}$	$\text{C}_{22}\text{H}_{26}\text{Cu}_2\text{N}_{10}\text{O}_2$
Molecular weight	850.65	775.76	1298.09	1277.24	589.61
Crystal system	Triclinic	Triclinic	Monoclinic	Orthorhombic	Monoclinic
Space group	$P\bar{1}$	$P\bar{1}$	$P2_1/n$	$P2_12_12_1$	$P2_1/c$
$a/\text{Å}$	8.739(5)	8.517(2)	18.275(2)	15.306(4)	10.8910(17)
$b/\text{Å}$	9.470(6)	9.409(5)	15.2381(18)	18.166(12)	9.2429(14)
$c/\text{Å}$	11.072(7)	10.910(3)	21.291(3)	19.200(6)	12.0176(19)
$\alpha/^\circ$	101.12(1)	102.85(4)	90.00	90.00	90.00
$\beta/^\circ$	108.20(1)	106.33(4)	96.189(2)	90.00	105.816(2)
$\gamma/^\circ$	95.57(1)	91.70(4)	90.00	90.00	90.00
$U/\text{Å}^3$	841.9(8)	814.0(8)	5894.5(12)	5339(4)	1163.9(3)
$D_c/\text{g cm}^{-3}$	1.678	1.583	1.451	1.589	1.682
Z	1	1	2	4	2
$F(000)$	438.00	402	2640	2640	604
Crystal size/mm	$0.21 \times 0.16 \times 0.02$	$0.40 \times 0.26 \times 0.18$	$0.28 \times 0.28 \times 0.04$	$0.42 \times 0.28 \times 0.22$	$0.25 \times 0.13 \times 0.05$
μ (mm^{-1})	1.493	1.375	1.582	1.652	1.871
Measured Reflections	5274	2852	11 571	5173	9099
θ range/ $^\circ$	2–27.5	2–24.96	2.61–23.72	1.54–24.96	1.94–28.28
R_1, wR_2 [$I > 2\sigma(I)$]	0.0688, 0.0734	0.0540, 0.1245	0.0667, 0.1515	0.0675, 0.1508	0.0461, 0.1104
hkl ranges	0,11;–12,12;–14,13	0,10;–11,11;–12,12	–22,22;–18,18;–26,26	0,18;0,21;0,22	–14,14;–11,12;–15,15
R_{int}	0.070	0.000	0.191	0.000	0.0467
Goodness-of-fit on F^2	1.537	1.028	0.967	1.036	1.002
Final difference map max., min./ $e\text{ Å}^{-3}$	1.20, –0.68	0.677, –0.403	0.858, –0.441	0.653, –0.974	0.906, –0.811

$$^a R_1 = \sum(|F_o| - |F_c|) / \sum |F_o|, wR_2 = [\sum w(|F_o| - |F_c|)^2 / \sum w(F_o)^2]^{1/2}, w = 0.75 / (\sigma^2(F_o) + 0.0010F_o^2).$$

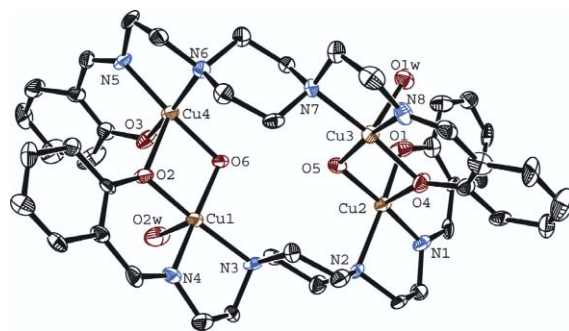
Table 2 Selected inter-atomic distances (Å) and angles (°) for complexes **1a** and **1b**

1a		1b	
Bond distances/Å			
Cu1–O1	1.875(7)	Cu1–O1	1.887(3)
Cu1–O2	1.947(6)	Cu1–N1	1.918(4)
Cu1–N1	1.910(8)	Cu1–N2	2.062(3)
Cu1–N2	2.060(8)	Cu1–O4	1.976(3)
Bond angles/°			
O1–Cu1–O2	91.1(3)	O1–Cu1–N1	94.08(15)
O1–Cu1–N1	94.2(3)	O1–Cu1–O4	90.40(13)
O1–Cu1–N2	177.9(4)	N1–Cu1–O4	161.93(17)
O2–Cu1–N1	165.8(3)	O1–Cu1–N2	177.05(18)
O2–Cu1–N2	88.7(3)	N1–Cu1–N2	85.75(15)
N1–Cu1–N2	86.4(3)	O4–Cu1–N2	88.88(13)

**Fig. 2** Packing diagram of **1b** viewed along the crystallographic *b* axis.

that the interaction of the metal with NO_3^- is stronger than with ClO_4^- . The $\text{Cu}\cdots\text{Cu}$ separations are 6.90 and 6.85 Å for **1a** and **1b**, respectively, whereas the shortest inter-metallic separations within the crystal are 4.46 and 4.73 Å, respectively. The layered layout of molecules of **1b** on the crystallographic *ab* plane (Fig. 2) illustrates the easy transformation of **1a** or **1b** into 1D azido bridged coordination polymers by replacement of the *cis* DMF and NO_3^- ligands on each copper by bridging N_3^- groups, thereby linking the dinuclear moieties into infinite chains, forming complex **4** (see below). Counter intuitively, this results into an increase of the $\text{Cu}\cdots\text{Cu}$ inter-dimer distance.

$[\text{Cu}_4(\text{L})_2(\text{OH})_2(\text{H}_2\text{O})_2]\text{X}_2$ ($\text{X} = \text{ClO}_4^-$, **2a**; NO_3^- , **2b**). Complex **2a** crystallizes in the $P2_1/n$ space group while complex **2b** crystallizes in the chiral $P2_12_12_1$ space group with absolute structure (Flack)²³ parameter of $-0.02(4)$, indicating the absolute structure of the molecules of **2b** in the crystal (see below). Both complexes exhibit the same cation, $[\text{Cu}_4(\text{L})_2(\text{OH})_2(\text{H}_2\text{O})_2]^{2+}$ (Fig. 3), where two L^{2-} ligands wrap an elongated tetrahedron of four Cu(II) centers in a helical manner. In a previous communication, complex **2a** was reported.¹⁵ Each ligand is hexadentate and coordinates one copper ion at each end, by means of one phenoxide, one imine and one piperazine moiety per metal, forming a $[\text{Cu}_2\text{L}]$ unit, similar to that exhibited by complexes **1a** and **1b**, now with

**Fig. 3** ORTEP representation at the 30% probability level of the complex cation $[\text{Cu}_4(\text{L})_2(\text{OH})_2(\text{H}_2\text{O})_2]^{2+}$ of **2b** (the cation of **2a** is almost identical). Hydrogen atoms are omitted for clarity. Only heteroatoms are labelled.

the piperazine moiety binding the metals in the *cis* fashion and adopting the a-e conformation (Scheme 2, C). The $[\text{Cu}_2\text{L}]$ units are connected by establishing two $[\text{Cu}_2\text{O}_2]$ pairs. The bridging O-atoms in each pair belong to one of the phenoxide units of L^{2-} and one OH^- group, respectively. The other phenoxide moiety of both L^{2-} ligands remains as a terminal group, completing five-coordination around two Cu(II) ions. The fifth coordination site of the other two metals is completed by two molecules of water. The Cu(II) ions in this complex exhibit thus N_2O_3 square pyramidal coordination environments, with axial positions occupied by either the water ligands (with bonds perpendicular to the $[\text{Cu}_2\text{O}_2]$ moieties) or μ -phenoxide groups (with bonds contained within the $[\text{Cu}_2\text{O}_2]$ fragments). The τ parameters of the coordination geometry are 0.02–0.08 for **2a** and 0.006–0.10 for **2b** (τ being equal to 1 for a pure trigonal bipyramid and to 0 for a square pyramid).²⁴ The coordination of the Cu ions by L^{2-} within the $[\text{Cu}_2\text{L}]$ units is therefore unsymmetrical (Figure S2).[†] The origin of this asymmetry is certainly the unequal coordination by the bidentate piperazine fragment, as a result of the a-e configuration. Selected bond distances and angles for complexes **2a** and **2b** are given in Tables 3 and 4, respectively. These tables reveal that complexes **2a** and **2b** represent two of the very rare examples displaying $[\text{Cu}_2\text{O}_2]$ moieties where, of the four bonds linking the metals, three are basal (short) and one axial (long). The relation between $\text{Cu}-\text{N}_{\text{am}}$ and $\text{Cu}-\text{N}_{\text{im}}$ distances is the same as for complexes **1a/b** (the first set being longer than the second one). The inter-metallic distances within the $[\text{Cu}_2\text{O}_2]$ pairs of complexes **2a/b** range from 3.09–3.10 Å, whereas the Cu metals separated by the piperazine moiety lay at average distances of 5.65 and 5.61 Å for **2a** and **2b**, respectively. The latter vectors are shorter than the equivalent distances for complexes **1a/b** (see above), which results from the difference of *trans* vs. *cis* coordination (Scheme 2, B vs C). Complexes **2a/b** display intramolecular hydrogen bonding between coordinated water molecules and the terminal phenoxide groups (Fig. S3).[†] The refinement of **2b** was performed anisotropically using full-matrix least-squares with all non-hydrogen atoms and hydrogens included on calculated positions, riding on their carrier atoms. The hydrogen positions of water molecules and hydroxyl groups O5 and O6 could not be determined. The disordered NO_3^- anions were refined isotropically over two positions with occupancy of 0.5 each. In complex **2a**, lattice and coordinated water molecules connect the $[\text{Cu}_4]$ units into chains *via* hydrogen bonds to the ClO_4^- anions (Fig. S4).[†]

Table 3 Selected inter-atomic distances (Å) and angles (°) for complexes **2a**

Bond distances/Å	
Cu1–N4	1.923(6)
Cu1–O6	1.924(5)
Cu1–O2	1.937(5)
Cu1–N3	2.083(6)
Cu2–O1	1.938(5)
Cu2–O5	1.945(4)
Cu2–N1	1.949(6)
Cu2–N2	2.159(6)
Cu2–O4	2.333(5)
Cu3–N8	1.890(7)
Cu3–O5	1.923(5)
Cu3–O4	1.951(5)
Cu3–N7	2.086(6)
Cu3–O15	2.296(7)
Cu4–O3	1.921(6)
Cu4–O6	1.940(5)
Cu4–N5	1.956(6)
Cu4–N6	2.177(6)
Cu4–O2	2.251(5)
Bond angles/°	
N4–Cu1–O6	172.1(3)
N4–Cu1–O2	93.8(2)
O6–Cu1–O2	82.8(2)
N4–Cu1–N3	85.1(2)
O6–Cu1–N3	97.4(2)
O2–Cu1–N3	172.8(3)
O1–Cu2–N2	171.0(2)
N8–Cu3–O4	92.8(3)
O5–Cu3–O4	84.5(2)
N8–Cu3–N7	83.5(3)
O5–Cu3–N7	97.5(2)
O4–Cu3–N7	167.7(2)
N8–Cu3–O15	98.5(3)
O5–Cu3–O15	89.3(3)
O4–Cu3–O15	97.3(2)
N7–Cu3–O15	94.9(3)
O3–Cu4–O6	87.7(2)
O3–Cu4–N5	91.4(3)
O6–Cu4–N5	171.3(2)
O3–Cu4–N6	170.4(3)
O6–Cu4–N6	96.7(2)
N5–Cu4–N6	83.0(3)
O3–Cu4–O2	94.1(2)
O6–Cu4–O2	74.66(19)
N5–Cu4–O2	114.1(2)
O5–Cu2–N2	97.2(2)
N1–Cu2–N2	83.0(2)
O1–Cu2–O4	94.6(2)
O5–Cu2–O4	74.42(19)
N1–Cu2–O4	115.0(2)
N2–Cu2–O4	94.2(2)
N8–Cu3–O5	172.0(3)
N6–Cu4–O2	95.3(2)

The structure of complex **2a** had been previously reported on a preliminary account of this work.¹⁵

The fact that complex **2b** crystallizes in a chiral space group means that this compound, present as a racemic mixture in solution, experiences spontaneous resolution upon crystallization. The origin of the chirality in this system, formed from achiral components, is the double helical configuration featured by the tetranuclear aggregates (Fig. 4). While the structure of one isomer of **2b** has been determined by single crystal X-ray diffraction

Table 4 Selected inter-atomic distances (Å) and angles (°) for complexes **2b**

Bond distances/Å	
Cu1–N4	1.936(12)
Cu1–O2	1.943(9)
Cu1–O6	1.938(9)
Cu1–N3	2.067(11)
Cu2–O5	1.920(10)
Cu2–O1	1.950(10)
Cu2–N1	1.967(12)
Cu2–N2	2.130(11)
Cu2–O4	2.338(10)
Cu3–O5	1.937(9)
Cu3–N8	1.947(12)
Cu3–O4	1.952(10)
Cu3–N7	2.092(12)
Cu4–N5	1.945(11)
Cu4–O6	1.942(9)
Cu4–O3	1.972(11)
Cu4–N6	2.143(12)
Cu4–O2	2.292(9)
O1W–Cu3	2.326(10)
O2W–Cu1	2.305(12)
Bond angles/°	
N5–Cu4–O6	174.2(5)
N5–Cu4–O3	91.4(5)
O6–Cu4–O3	86.4(4)
N5–Cu4–N6	83.4(5)
O6–Cu4–N6	97.7(4)
O3–Cu4–N6	168.0(4)
N5–Cu4–O2	110.7(4)
O6–Cu4–O2	75.0(3)
O3–Cu4–O2	96.8(4)
N6–Cu4–O2	95.2(4)
O5–Cu3–N8	168.6(5)
O5–Cu3–O4	83.8(4)
N8–Cu3–O4	92.0(5)
O5–Cu3–N7	97.2(4)
N8–Cu3–N7	85.5(5)
O4–Cu3–N7	172.1(5)
O5–Cu3–O1W	90.3(4)
N8–Cu3–O1W	100.4(4)
O4–Cu3–O1W	92.0(4)
N7–Cu3–O1W	95.8(4)
N4–Cu1–O2	92.5(5)
N4–Cu1–O6	169.0(5)
O2–Cu1–O6	83.8(4)
N4–Cu1–N3	84.5(5)
O2–Cu1–N3	169.4(5)
O6–Cu1–N3	97.3(4)
N4–Cu1–O2W	100.3(5)
O2–Cu1–O2W	96.6(5)
O6–Cu1–O2W	90.4(4)
N3–Cu1–O2W	94.0(5)
O5–Cu2–O1	88.1(4)
O5–Cu2–N1	172.8(5)
O1–Cu2–N1	91.0(5)
O5–Cu2–N2	95.7(4)
O1–Cu2–N2	169.3(5)
N1–Cu2–N2	84.0(5)
O5–Cu2–O4	74.4(4)
O1–Cu2–O4	96.0(4)
N1–Cu2–O4	112.8(4)
N2–Cu2–O4	94.6(4)
Cu1–O2–Cu4	93.4(4)
Cu4–O6–Cu1	105.6(4)
Cu3–O4–Cu2	92.3(4)
Cu2–O5–Cu3	107.3(5)

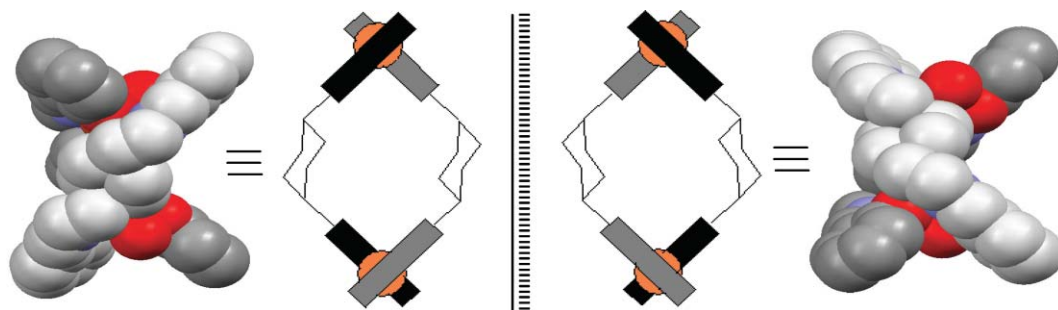


Fig. 4 Space-filling and schematic representation of the two isomeric forms of complex **2b**. Left, P helix; Right, M helix.

(P helix), the presence of the other one (M helix)²⁵ was confirmed from circular dichroism spectroscopy (see below). Interestingly, the space group of **2a** is not chiral because both isomers of this complex co-crystallize and are therefore contained within the unit cell of the crystal lattice.

[Cu₂L(N₃)₂]_n (4). The structure of **4** consist of an infinite chain along the crystallographic *b* axis of [Cu₂L(N₃)₂] repeating units (Fig. 5), each involving one L²⁻ hexadentate ligand that acts as a bridge between two symmetry equivalent Cu(II) ions in the same manner as in complexes **1a/b** (thus, in a *trans*-e,e fashion, Scheme 2, A). Each metal ion displays a N₃⁻ ligand at its fourth equatorial position. The azido ligands link the [Cu₂L] moieties to each other (Fig. 6 and S5)[†] by completing the square pyramidal geometry ($\tau = 0.186$) of the Cu(II) ions from a neighbouring dinuclear fragment, thereby featuring the end-to-end basal-apical bridging coordination mode. The resulting chain thus exhibits double azido bridges, in form of [Cu(μ -1,3-N₃)₂Cu] moieties that constitute eight-member rings in a chair conformation where the six nitrogen atoms are contained in the same plane (Figure S6).[†] The angle between this plane and the N3–Cu1–N5 plane is 48.4°, while the Cu1–N3–N5–Cu1* (* = 1 - *x*, -*y*, 2 - *z*) torsion angle is 72.69°. The Cu...Cu distance across the piperazine bridge is 6.83 Å, whereas the Cu(II) ions separated by the double azido bridge lie much closer to each other (4.77 Å). Selected bond lengths and angles involving the metal centers in this complex are listed in Table 5. The chains occur with a period of 4.45 Å along the crystallographic *c* axis (Figure S7),[†] which is a shorter distance than the Cu...Cu separations within the chains.

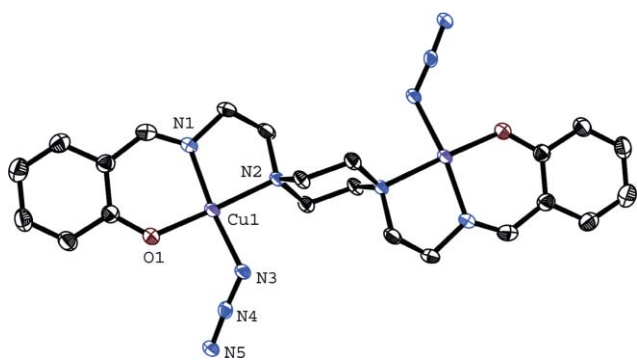


Fig. 5 ORTEP representation at the 40% probability level of the repeating unit of the coordination polymer [Cu₂L(N₃)₂]_n (**4**). Hydrogen atoms are omitted for clarity. Only independent non-carbon atoms are labelled.

Table 5 Selected inter-atomic distances (Å) and angles (°) for complex **4**

Bond distances/Å	
Cu1–O1	1.900(2)
Cu1–N1	1.955(3)
Cu1–N3	1.973(3)
Cu1–N2	2.067(3)
Bond angles/°	
O1–Cu1–N1	93.03(12)
O1–Cu1–N3	91.29(12)
N1–Cu1–N3	165.11(14)
O1–Cu1–N2	176.31(11)
N1–Cu1–N2	84.69(12)
N3–Cu1–N2	90.21(11)

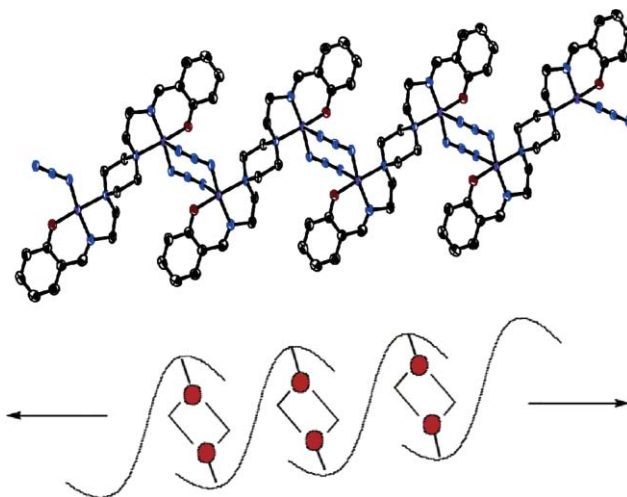


Fig. 6 (Top) ORTEP representation at the 40% probability level of the coordination polymer [Cu₂L(N₃)₂]_n (**4**), hydrogen atoms are omitted for clarity and (bottom) schematic representation of the assembly of emphasizing how the *trans* configuration of L²⁻ favours the formation of a chain instead of discrete dimeric entities.

Piperazine conformations and coordination modes. The diversity of the above structures may be observed, in part, thanks to the versatility in conformation and stereochemistry of coordination of the piperazine backbone (Fig. S8).[†] Thus, as free ligand, in the solid-state, this molecule is present in the chair-a,a conformation. Coordination to Cu(II) triggers a change of the stereochemistry,

with the inversion in orientation of the N-atom lone pairs, thus leading to the *e,e* conformation (complexes **1a/b** and **4**). Certain reaction conditions favour the adoption of a *cis* configuration upon coordination of two copper ions (presumably to allow the dimerization into a [Cu₄] species) thereby unveiling the rare *a,e* form of piperazine.

Circular dichroism of **2b**

Complex **2b**, which is formed from achiral components, crystallizes in a chiral space group (see above). The chirality originates from the double helical binding mode of the ligand L²⁻. Interestingly, the complex **2b** with NO₃⁻ salt crystallizes as a racemate. Circular dichroism (CD) spectral measurements helped to understand the optical properties of these complexes. Thus, a single crystal of **2b** was selected and dissolved in MeCN for CD spectroscopy. The spectrum in the 200–300 nm wavelength range (Fig. 7, left) reveals positive and negative Cotton effects with λ_{max} = 263 and 230 nm, respectively, which compares well with the electronic absorption spectrum of **2b** (Fig. 7, right). This CD spectrum is consistent with the chiral nature of the single crystals of **2b**. A polycrystalline sample was also dissolved in MeCN and the solution produced an unresolved CD pattern (Fig. 7). This confirms the fact that complex **2b** experiences spontaneous chiral resolution upon crystallization, and that single crystals from both enantiomers are present in a polycrystalline sample of the compound. The fact that an unresolved pattern is observed likely reveals the occurrence of an enantiomeric excess (ee) in the chosen mixture. Nevertheless, the observation of opposite Cotton effect at the wavelength 230 nm provides definitive evidence for presence of both isomers in the polycrystalline mixture of **2b**.

Bulk magnetization measurements

The magnetic properties of the above family of compounds are discussed in light of bulk magnetization measurements. All compounds consist of [Cu₂L] fragments with Cu(II) centers (*S* = 1/2) bridged by a piperazine bridge. One interesting thing is to compare the efficiency of the magnetic coupling by piperazine in different conformations.

The magnetic properties of complexes **1a/b** and **2a/b** have been previously communicated by some of us,^{13,15} therefore, only a summary is presented here. Compound **4** has been studied now for the first time and the complete analysis is reported in this manuscript.

Variable-temperature susceptibility measurements on complex **1a** showed that the Cu(II) ions connected by L²⁻ experience antiferromagnetic exchange coupling *via* the *trans-e-e* piperazine bridge.¹³ The $\chi_{\text{M}}T$ vs. *T* curve was fit to a model function and the coupling constant was found to be *J* = -14.1 cm⁻¹ (using the Hamiltonian $H = -2JS_1S_2$), in line with other systems exhibiting the same type of bridge.²⁶ The coupling was postulated to occur *via* the σ -bonding backbone of the piperazine ring, since the σ -type orbitals of this fragment have the appropriate symmetry to interact directly with dx² - y² magnetic orbitals of Cu(II).

The tetranuclear complex **2a** was also studied through bulk magnetization measurements. This system exhibits two types of magnetic interaction, one mediated by the piperazine ring of L²⁻ and one occurring within the [Cu₂(μ -O)₂] moiety (as mediated by a hydroxide and a phenoxide group). Fitting of the $\chi_{\text{M}}T$ vs. *T* curve through a full diagonalization procedure revealed that the coupling through both types of pathways are very similar.¹⁵ Coupling constants of *J*₁ = *J*₂ = -16.2 cm⁻¹ were determined by considering the Hamiltonian $H = -2J_1(S_1S_2 + S_3S_4) - 2J_2(S_1S_4 + S_2S_3)$, where Fig. 5 may be used for the labels of the spin centers. The piperazine group in **2a** is linking the Cu(II) ions in the very rare *trans-a-e* fashion. This conformation allows for two mechanisms of the exchange interaction; (i) through the σ -bonding framework, (ii) through-space, *via* direct N-to-N delocalization, involving the lone pairs of nitrogen.²⁷ Interestingly, the difference in conformation of the piperazine group in complexes **1a** and **2a** does not represent a significant variation in magnitude of the exchange interaction. On the other hand, the interaction mediated by two μ -O atoms occurs through a very rare combination of three basal (short) and one apical (long) Cu–O bonds. In the very few cases where this has been found and studied, the observed coupling constants range -11 to -19 cm⁻¹.^{28,29}

Variable-temperature magnetic susceptibility measurements were performed on complex **4** in the 2–300 K range under a constant field of 1 T. The resulting $\chi_{\text{M}}T$ vs. *T* plot (Fig. 8)

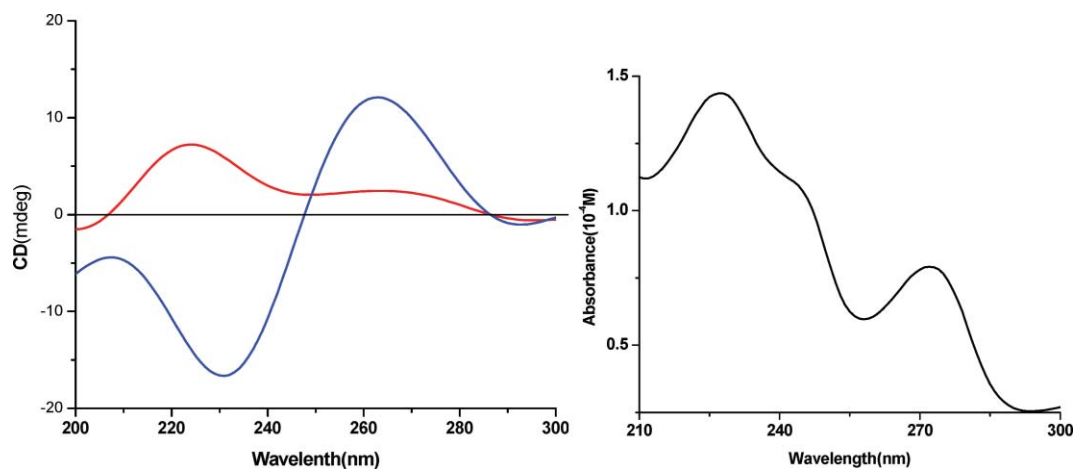


Fig. 7 Left; CD spectrum of a single crystal of **2b** in MeCN solution (blue line) and unresolved CD spectrum of polycrystalline mixture of **2b** in MeCN solution (red line). Right, UV-vis spectrum of complex of **2b** in MeCN solution.

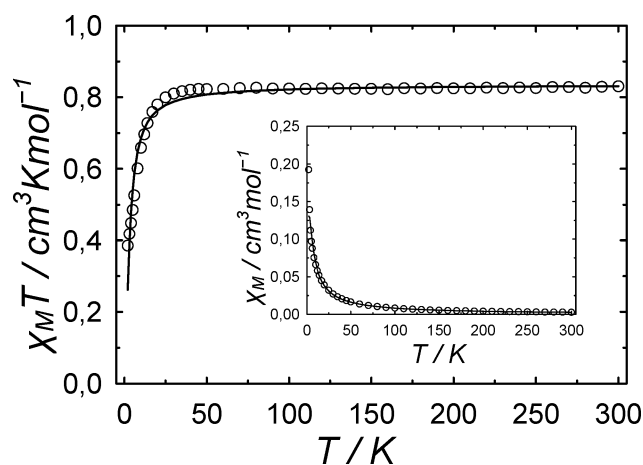


Fig. 8 Plot of $\chi_M T$ vs. T per mole of complex **4**. The solid line is a fit to the appropriate $\chi_M = f(T)$ model function (see text for details). The inset is the χ_M vs. T representation and the corresponding fit.

exhibits a constant value of the $\chi_M T$ product, which only drops at low temperatures (~ 50 K), revealing the presence of weak antiferromagnetic interactions within the chain. The topology of the spin carriers within the coordination polymer **4** corresponds to that of a uniform alternate chain (two types of magnetic interactions that alternate along the chain) and thus, described by the Hamiltonian $H = -2J_1 \sum S_{2i} S_{2i-1} - 2J_2 \sum S_{2i} S_{2i+1}$ ($i = 1$ to $n/2$) where S_i is the spin of a Cu(II) ion ($S = 1/2$). An expression for the $\chi_M = f(T)$ function has been previously deduced for this system,³⁰ and was used to fit the experimental data. The best simulation (Fig. 8, solid line) was obtained for the following parameters; $J_1 = -1.33$, $J_2 = -1.20$ and $g = 2.11$. Since both coupling constants are so similar, it is futile to attempt to assign them to each type of magnetic coupling pathway. The coupling occurring through the bridging $\mu_{1,3}\text{-N}_3^-$ groups is expected to be antiferromagnetic, and very weak. It is well established that, with very rare exceptions,^{31,32} end-to-end azido bridges mediate antiferromagnetic interactions.¹ On the other hand, each bridging ligand is bound to one Cu(II) ion at its apical position, thereby experiencing very small overlap with the magnetic orbital ($dx^2 - y^2$) of this metal. It is noteworthy, however, the weak nature of the coupling through the piperazine group, as compared with previously characterized similar examples (for example, one order of magnitude smaller than in complex **1a**). Since the geometry of all the Cu(II) pairs bridged by *trans*-e,e piperazine are very similar, the reason for the difference in magnetic couplings might lie on the presence of complementary or counter-complementary effects caused by the various ligands bound to the paramagnetic centers.³³ The slight divergence of the fit at the lowest temperatures (below 5 K) are most likely due to a small amount of paramagnetic impurity, which is particularly visible in this regime of antiferromagnetically coupled systems.

X-Ray crystallography

Information concerning X-ray data collection and structure refinement of the compound is summarized in Table 1. The intensity data of the complexes **1a**, **2a** and **4** were collected in Bruker SMART CCD single-crystal X-ray diffractometer and that of **1b** and **2b** were collected on Nonius CAD4 X-ray diffractometer that

uses graphite monochromated MoK α radiation ($\lambda = 0.71073$ Å) by ω -scan method. Data were collected at 305, 298 and 100 K for complexes **1a**, **2a** and **4**, respectively whereas for complexes **1b** and **2b**, data were collected at 293 K. In the final cycles of full-matrix least-squares on F^2 all non-hydrogen atoms were assigned anisotropic thermal parameters. The structure was solved using the programme SHELX-97³⁴ and refined by full-matrix least squares methods with use of the programme SHELX-97.³⁵

Conclusions

The study of the coordination chemistry of the piperazine containing ligand H_2L has revealed a change in conformation of the heterocycle upon coordination, going from a,a to *trans*-e,e (complexes **1a/b** and **4**) or to the unprecedented *cis*-a,e mode (complexes **2a/b** and postulated for **3a/b**). The presence and type of bridging co-ligands (OH^- or N_3^-) seem to define the conformation adopted by the piperazine bridge, depending on the requirements of the preferred complex. As a result, various topologies for the coordination assemblies have emerged, namely, piperazine bridged Cu(II) discrete dimers (**1a/b**), tetranuclear complexes with an elongated tetrahedral $[Cu_4]$ arrangement (**2a/b** and presumably **3a/b**) or an infinite succession of $[Cu_2L]$ fragments linked by double end-to-end azido bridges. Complexes **2a/b** exhibit chirality (from achiral components) resulting by the helical arrangement of the L^{2-} ligands around the metals. Interestingly, in complex **2b**, spontaneous resolution of the racemic mixture present in solution after its formation occurs upon crystallization. Thus, the product exhibits a chiral space group, and as a result, single crystals of complex **2b** display optical activity. All possible magnetic pathways identified in these compounds have revealed themselves to be weakly antiferromagnetic. Interestingly, an order of magnitude of difference has been observed between two cases of the *trans*-e,e bridge by piperazine. This is attributed to differences in complementary effects between the various ligands of the metal ions.

Acknowledgements

We are thankful to the Council of Scientific and Industrial Research, New Delhi, for the financial support. We also thank DST, New Delhi, for the Single-Crystal X-ray Diffractometer facility in the Department of Chemistry, IIT Kharagpur under its FIST program. J. L. and G. A. acknowledge the financial supports from the Governments of the US and Spain, respectively. We thank Dr V. Bertolasi, Dipartimento di Chimica e Centro di Strutturistica Diffraattometrica, Università di Ferrara, via L. Borsari, 46, 44100 Ferrara, Italy, for his kind help.

Notes and references

- J. Ribas, A. Escuer, M. Monfort, R. Vicente, R. Cortes, L. Lezama and T. Rojo, *Coord. Chem. Rev.*, 1999, **195**, 1027–1068.
- J. A. Real, A. B. Gaspar, V. Niel and M. C. Munoz, *Coord. Chem. Rev.*, 2003, **236**, 121–141.
- E. Coronado, J. R. Galán-Mascarós, C. J. Gómez-García and V. Laukhin, *Nature*, 2000, **408**, 447–449.
- J. Rättiläinen, K. Airola, R. Frohlich, M. Nieger and K. Rissanen, *Polyhedron*, 1999, **18**, 2265–2273.
- K. Rissanen, J. Breitenbach and J. Huuskonen, *J. Chem. Soc., Chem. Commun.*, 1994, 1265–1266.

- 6 K. Airola, J. Ratilainen, T. Nyronen and K. Rissanen, *Inorg. Chim. Acta*, 1998, **277**, 55–60.
- 7 M. Boiocchi, M. Bonizzoni, L. Fabbrizzi, F. Foti, M. Licchelli, A. Taglietti and M. Zema, *Dalton Trans.*, 2004, 653–658.
- 8 U. Mukhopadhyay and I. Bernal, *Cryst. Growth Des.*, 2006, **6**, 363–365.
- 9 Z. Smekal, Z. Travnicek, J. Mrozinski and J. Marek, *Inorg. Chem. Commun.*, 2003, **6**, 1395–1399.
- 10 S. S. Massoud and F. A. Mautner, *Inorg. Chem. Commun.*, 2004, **7**, 559–562.
- 11 B. Chiari, O. Piovesana, T. Tarantelli and P. F. Zanazzi, *Inorg. Chem.*, 1984, **23**, 3398–3404.
- 12 B. Chiari, O. Piovesana, T. Tarantelli and P. F. Zanazzi, *Inorg. Chem.*, 1982, **21**, 1396–1402.
- 13 M. Bera, J. Ribas, W. T. Wong and D. Ray, *Inorg. Chem. Commun.*, 2004, **7**, 1242–1245.
- 14 B. Chiari, O. Piovesana, T. Tarantelli and P. F. Zanazzi, *Inorg. Chem.*, 1984, **23**, 2542–2547.
- 15 A. R. Paital, P. K. Nanda, S. Das, G. Aromí and D. Ray, *Inorg. Chem.*, 2006, **45**, 505–507.
- 16 M. C. Suen, T. C. Keng and J. C. Wang, *Polyhedron*, 2002, **21**, 2705–2710.
- 17 L. Carlucci, G. Ciani, D. M. Proserpio and A. Sironi, *Inorg. Chem.*, 1995, **34**, 5698–5700.
- 18 J. Mendham, R. C. Denney, J. D. Barnes, M. J. K. Thomas, *Vogel's Textbook of Quantitative Chemical Analysis*, 3rd edn., 2007, p 462.
- 19 F. Chuburu, R. Tripier, M. Le Baccon and H. Handel, *Eur. J. Org. Chem.*, 2003, 1050–1055.
- 20 M. Bera, W. T. Wong, G. Aromí, J. Ribas and D. Ray, *Inorg. Chem.*, 2004, **43**, 4787–4789.
- 21 G. Aromí, P. Gamez, O. Roubeau, P. C. Berzal, H. Kooijman, A. L. Spek, W. L. Driessen and J. Reedijk, *Inorg. Chem.*, 2002, **41**, 3673–3683.
- 22 B. Graham, M. T. W. Hearn, P. C. Junk, C. M. Kepert, F. E. Mabbs, B. Moubaraki, K. S. Murray and L. Spiccia, *Inorg. Chem.*, 2001, **40**, 1536–1543.
- 23 H. D. Flack, *Acta Crystallogr., Sect. A: Found. Crystallogr.*, 1983, **39**, 876–881.
- 24 A. W. Addison, T. N. Rao, J. Reedijk, J. Vanrijn and G. C. Verschoor, *J. Chem. Soc., Dalton Trans.*, 1984, 1349–1356.
- 25 V. Amendola, L. Fabbrizzi, C. Mangano, P. Palavicini, E. Roboli and M. Zema, *Inorg. Chem.*, 2000, **39**, 5803–5806.
- 26 P. S. Mukherjee, S. Dalai, G. Mostafa, E. Zangrando, T. H. Lu, G. Rogez, T. Mallah and N. R. Chaudhuri, *Chem. Commun.*, 2001, 1346–1347.
- 27 B. Chiari, O. Piovesana, T. Tarantelli and P. F. Zanazzi, *Inorg. Chem.*, 1984, **23**, 2542–2547.
- 28 M. Koikawa, H. Yamashita and T. Tokii, *Inorg. Chim. Acta*, 2004, **357**, 2635–2642.
- 29 G. Cros, J. P. Laurent and F. Dahan, *Inorg. Chem.*, 1987, **26**, 596–599.
- 30 J. W. Hall, W. E. Marsh, R. R. Weller and W. E. Hatfield, *Inorg. Chem.*, 1981, **20**, 1033–1037.
- 31 C. S. Hong, J. E. Koo, S. K. Son, Y. S. Lee, Y. S. Kim and Y. Do, *Chem.–Eur. J.*, 2001, **7**, 4243–4252.
- 32 T. K. Maji, P. S. Mukherjee, G. Mostafa, T. Mallah, J. Cano-Boquera and N. R. Chaudhuri, *Chem. Commun.*, 2001, 1012–1013.
- 33 M. S. El Fallah, F. Badyine, R. Vicente, A. Escuer, X. Solans and M. Font-Bardia, *Dalton Trans.*, 2006, 2934–2942.
- 34 G. M. Sheldrick, *SHELXS-97, Program for solution of crystal structures*, University of Göttingen, Germany, 1997.
- 35 G. M. Sheldrick, *SHELXL-97, Program for refinement of crystal structures*, University of Göttingen, Germany, 1997.